# Extreme Cold Outbreaks in the United States and Europe, 1948–99

JOHN E. WALSH, ADAM S. PHILLIPS,* DIANE H. PORTIS, AND WILLIAM L. CHAPMAN

*Department of Atmospheric Sciences, University of Illinois at Urbana–Champaign, Urbana, Illinois*

## ABSTRACT

Reanalysis output for 1948–99 is used to evaluate the temporal distributions, the geographical origins, and the atmospheric teleconnections associated with major cold outbreaks affecting heavily populated areas of middle latitudes. The study focuses on three subregions of the United States and two subregions of Europe. The cold outbreaks affecting the United States are more extreme than those affecting Europe, in terms of both the regionally averaged and the local minimum air temperatures. There is no apparent trend toward fewer extreme cold events on either continent over the 1948–99 period, although a long station history suggests that such events may have been more frequent in the United States during the late 1800s and early 1900s. The trajectories of the coldest air masses are southward or southeastward over North America, but westward over Europe. Subsidence of several hundred millibars is typical of the trajectories of the coldest air to reach the surface in the affected regions. Sea level pressure anomalies evolve consistently with the trajectories over the 1–2 weeks prior to the extreme outbreaks, and precursors of the cold events are apparent in coherent antecedent anomaly patterns. Negative values of the North Atlantic oscillation index and positive anomalies of Arctic sea level pressure are features common to North American as well as European outbreaks. However, the strongest associated antecedent anomalies of sea level pressure are generally shifted geographically relative to the nodal locations of the North Atlantic and Arctic oscillations.

## 1. Introduction

Extreme cold-air outbreaks affect larger numbers of midlatitude residents than other types of severe weather such as tornadoes and hurricanes. While concern about cold outbreaks runs counter to the popular notion of global warming, population growth and more complex transportation systems make the midlatitudes increasingly vulnerable to extreme outbreaks of cold air (Witten 1981). Moreover, the changes of atmospheric circulation that may accompany future global warming are highly uncertain, leaving open the possibility that the severity of cold outbreaks in middle latitudes may not decrease as the global mean temperature increases. In the present paper, we address the frequencies, origins, and atmospheric teleconnections associated with cold air outbreaks affecting the United States and Europe. One of our primary goals is to assess the linkage between these severe cold outbreaks and the large-scale hemispheric circulation. A particular focus will be the preoutbreak evolution of the near-surface atmosphere in the Arctic

and subarctic. As a hemispheric heat sink, the northern high latitudes play a central role in the attainment of the extremely low temperatures that can affect the middle latitudes.

## 2. Relation to previous work

While many studies have addressed cold surges associated with the Asian monsoon (cf. Joung and Hitchman 1982), the present study will focus on the coldest airmasses affecting the United States and Europe. For the United States, Wexler (1951) was among the first to address in a systematic way the characteristics of cold or polar anticyclones, which result from a combination of mass convergence, diabatic cooling, and cold air advection. Individual outbreaks have been examined by Wagner (1977), Quiroz (1984), and Mogil et al. (1984), among others. Composites of several anticyclones originating in the northwestern Canada–Alaska region were constructed by Dallavalle and Bosart (1975), although their study emphasized the eventual fate of the anticyclones after their southward migration over the United States. Colucci and Davenport (1987) compiled a synoptic climatology of rapid anticyclogenesis events over North America and the adjacent oceans during one year. Many of the cold-season anticyclogenesis events in western North America were followed by cold-air outbreaks, although none were in the ''record-setting'' cat-

* Current affiliation: National Center for Atmospheric Research, Boulder, Colorado.

*Corresponding author address:* John E. Walsh, Department of Atmospheric Sciences, University of Illinois at Urbana–Champaign, 105 S. Gregory Avenue, Urbana, IL 61801.
E-mail: walsh@atmos.uiuc.edu

egory addressed in the present paper. In a diagnosis of two major 1977 outbreaks over North America, Konrad and Colucci (1989) focused on cold advection, adiabatic warming (subsidence) or cooling, and upstream cyclones. Their results suggested that the intensity of the cold air outbreaks varies with the size of the area of cold advection and with the timing of the associated cyclogenesis. Colle and Mass (1995) examined cold air surges east of the Rocky Mountains by diagnosing the momentum, energy, and vorticity budgets in a case study. A composite analysis included in that study pointed to the importance of interactions between synoptic systems and the topography of the western United States. Colucci et al. (1999) used an ensemble of numerical model forecasts to infer that nonadiabatic processes appear to have played a key role in the intensification of at least one extreme cold outbreak affecting the United States in 1985. Colucci et al.'s results left open the possibility that radiative cooling may be enhanced by the presence of low-level condensate, including clouds and clear-sky ice crystal precipitation (Curry 1983, 1987). Kalkstein et al. (1990) used synoptic data from four stations in Alaska and northwestern Canada to infer that the coldest air masses in this source region were somewhat less frequent and less cold in the 1970s and 1980s than in earlier decades. This finding does not, however, preclude quite different temporal variability of the extreme cold outbreaks that reach the midlatitude areas of North America.

Several studies during the past decade have addressed cold air outbreaks in the context of Florida citrus freezes. Rogers and Rohli (1991) showed that such freezes tend to occur in clusters, for example, the 1890s and 1977–89. Rogers and Rohli showed that major freeze events in Florida have tended to be associated with the positive phase of the atmospheric Pacific–North American (PNA) teleconnection pattern, as did Downton and Miller (1993). Downton and Miller also included the Southern Oscillation index and the North Atlantic oscillation index in a statistical comparison with monthly mean and monthly mean minimum temperatures in central Florida.

More recently, DeGaetano (1996) showed a tendency toward fewer cold minimum temperature threshold exceedences in the northeastern United States over the 1959–93 period. This tendency appears to be part of a broader trend toward higher minimum temperatures over the United States during the past half-century (Karl et al. 1991; Easterling et al. 2000). However, for the more recent period since 1975, Kunkel et al. (1999) report an absence of trends in fatalities and citrus damage due to cold waves in the United States.

For much of Europe, wintertime minimum temperatures have also been increasing more rapidly than the maximum temperatures (Brázdil et al. 1996; Heino et al. 1999). However, there have been suggestions that the occurrence of extremely cold winter conditions in Great Britain may have increased during the late 1970s and 1980s (Thompson 1987), and the 1990s have also seen occasional episodes of extreme cold (Brugge 1991). Nevertheless, the overall tendency toward milder winters appears in the temperature data for much of Europe, and this tendency is at least partially attributable to the predominance of the positive phase of the North Atlantic oscillation (NAO) during the 1980s and 1990s (Hurrell and van Loon 1997; Thompson and Wallace 1998). The fact that the NAO modulates the intensity of maritime airflow into much of Europe suggests that the NAO will play a role in the susceptibility of Europe to cold outbreaks, although the most appropriate timescale for delineating this association has not been established. Furthermore, the NAO has been shown by Thompson and Wallace to be part of a broader hemispheric pattern of atmospheric variability, the so-called Arctic oscillation. The extension of this mode to high latitudes gives it a potential role in the evolution of extreme air masses affecting North America as well as Europe.

The study described here will draw upon atmospheric fields for 1948–99 from an atmospheric reanalysis, which provides a consistent set of temperature and circulation fields for all middle and high-latitude areas. The availability of the reanalysis output permits 1) the identification of extreme cold events on a region-wide basis, and 2) a systematic comparison of low-temperature extreme events in different regions and from different decades of the past half-century. In addition to permitting an assessment of the temporal variability of extreme cold events on a regional basis, the reanalysis output permits an evaluation of the atmospheric circulation anomalies that precede major cold air outbreaks. We are thus able to address the geographical origins, the evolution and the atmospheric teleconnections associated with extreme cold events in different regions. Our focus on these aspects is intended to provide a broader perspective on the cold events than has emerged from the studies summarized above.

Section 3 is a summary of the relevant reanalysis data. In section 4, we discuss the procedure by which the coldest events are identified for various regions in the United States and Europe. The temporal distribution of the extreme outbreaks in the various regions is summarized in section 5, while section 6 addresses the geographical origins of the cold outbreaks in terms of trajectories, antecedent atmospheric circulation anomalies, and the teleconnection patterns associated with events affecting the different geographical regions. While earlier studies of teleconnections (e.g., Downton and Miller 1993) used monthly and/or seasonally averaged quantities to assess atmospheric linkages, our analysis in sections 4–6 is based on daily data to capture better the extreme excursions that occur on shorter timescales. In particular, our diagnostic analysis is intended to identify 1) the relevant timescale of the evolution of a major cold outbreak and 2) the associated spatial characteristics at the various stages of evolution. In this respect,
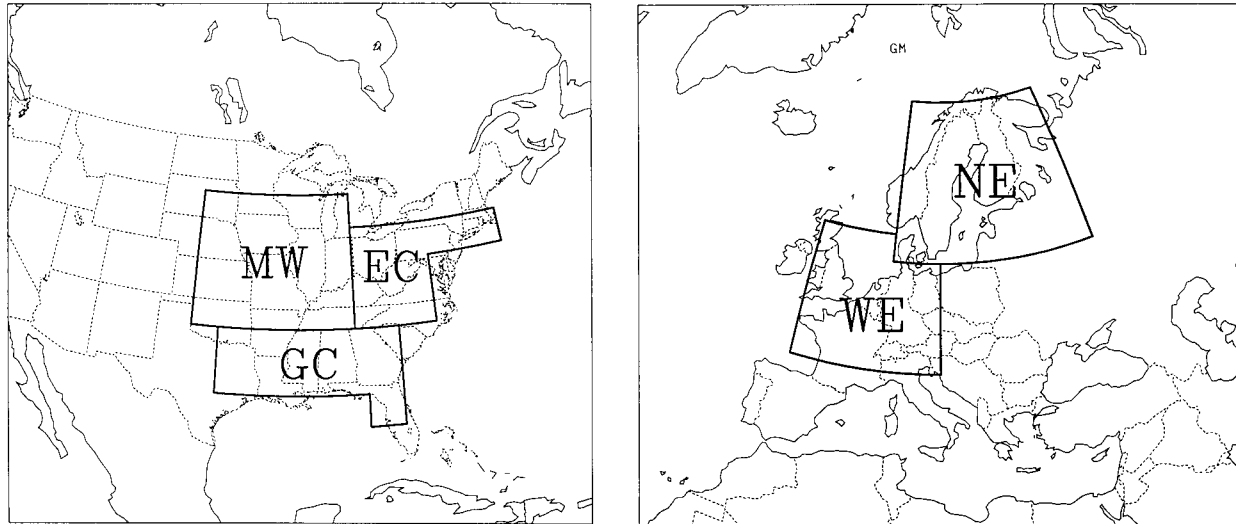
FIG. 1. The three North American regions and two European regions for which extreme cold events were identified.

the present work extends the synoptic climatological study of Konrad (1996), who correlated cold-air outbreaks over the southeastern United States to the atmospheric circulation over North America.

## 3. Data summary

The dataset used here was the gridded output of the atmospheric reanalysis performed by the National Centers for Environmental Prediction–National Center for Atmospheric Research (NCEP–NCAR). The NCEP–NCAR 40-Year Reanalysis is described by Kalnay et al. (1996). The output used here consisted of $4\times$-daily grids provided by the National Oceanic and Atmospheric Administration/Cooperative Institute for Research in Environmental Science (NOAA/CIRES) Climate Diagnostics Center, Boulder, Colorado (http://www.cdc.noaa.gov). The grids have a horizontal resolution of 2.5° lat × 2.5° long. The reanalysis begins in January 1948 and extends to the present; out study period ends in December 1999, resulting in a 52-yr period of record. The fields used here are the surface air temperatures (from the lowest model level, $\sigma = 0.995$), the sea level pressure and the three-dimensional upper-air winds (for the trajectory computations in section 5). In the cases of the surface air temperatures and sea level pressures, the $4\times$-daily values were averaged into daily grids. The four daily grids of wind for each day were retained for the trajectory computations. We note that a second reanalysis, performed by the European Centre for Medium-Range Weather Forecasts (ECMWF) is also available for years 1979–93. Although the shorter period of the ECMWF reanalysis limits its utility in a study such as the present one, we have compared the relevant outputs from the two reanalyses. The comparison of surface air temperatures is summarized below.

While the temperatures, pressures and wind fields are based on observational data assimilated directly into the reanalysis, other model-derived fields such as radiative fluxes, cloudiness, and sensible and latent heat fluxes are available in the reanalysis output archive. However, these model-derived variables have much larger uncertainties than the assimilated variables (e.g., Walsh and Chapman 1998) and hence are not included in the present study.

## 4. Event identification and sensitivities

The extreme cold events were identified for five heavily populated regions, three in the United States (MW = Midwest, EC = East Coast, GC = Gulf Coast) and two in Europe (NE = Northern Europe, WE = Western Europe). Figure 1 shows the boundaries of these regions as they have been defined here; the shapes of the boundaries are constrained by the 2.5° × 2.5° resolution of the reanalysis output. The three regions in the United States are east of the Rocky Mountains, so they are all susceptible to cold polar air masses that are often constrained on the west by the Rocky Mountain range as they slide southeastward. Indeed, the three regions share some (but not all) of the same extreme events. Of the two European regions, the mountains of Norway are the major orographic feature of NE, while the Alps are the only major mountain range in WE. The latter region includes Great Britain as well as a large portion of the North Sea, while NE includes the Baltic Sea. The MW, EC, and GC regions of the United States consist almost entirely of land and are smaller than the European regions. The respective regional areas are 1.77 × 10⁶ km² (MW), 1.07 × 10⁶ km² (EC), 0.99 × 10⁶ km² (GC), 3.47 × 10⁶ km² (NE), and 2.47 × 10⁶ km² (WE).

The extreme cold events for each region were defined on the basis of the daily surface air temperature anom-

alies averaged over the region. All anomalies are relative to the daily means (i.e., 52-yr average) for the calendar date and region. The daily means for a region were obtained using the 52-yr averages of the daily values for all grid points in the region. The spatial averaging was performed by summing the gridpoint anomalies in a region and dividing by the number of grid points. Since the actual areas varied from region to region, we examined the sensitivity to domain size by repeating the procedure for one region in three different sizes. The final selections of cases were virtually identical, although the relative ranks of the selected events did show some changes.

Once a date was selected, the antecedent and subsequent 10 days were eliminated from the search for additional extreme dates in the same region. In order to address the sensitivities of the selection procedure to the duration of the extreme cold event, the procedure was repeated after replacing each daily regional anomaly by a 3-day centered average of the anomaly and by a 5-day centered average of the anomaly. The use of the temporally averaged anomalies gives slightly more weight to events in which the extreme cold persisted in the same region for more than one or two days.

Prior to discussing the temporal distribution of the cold events in each region, we note a concern about a possible inhomogeneity of the NCEP reanalysis because of the introduction of satellite data. While the introduction of satellite data should impact the upper-air fields more than the surface fields used here, we nevertheless split the reanalysis output into 1948–78 and 1979–99 periods in order to address possible impacts of the introduction of satellite data. The calendar-month means and standard deviations of the regional daily temperatures were found to show no systematic differences between the pre- and post-1979 periods. For example, the monthly mean temperatures for 1948–78 (1979–99) in the EC region of the United States were 6.7°C (7.0°C) for November; 1.1°C (1.1°C) for December; −0.9°C (−0.9°C) for January; 0.5°C (0.7°C) for February; and 4.8°C (5.0°C) for March. The corresponding standard deviations of the daily temperatures in the EC region were 5.2°C (4.8°C) for November; 5.6°C (5.8°C) for December; 6.1°C (5.6°C) for January; 5.5°C (5.7°C) for February; and 5.1°C (5.2°C) for March. In no region or month did the mean temperatures of the two periods differ by more than 1°C, nor did any standard deviation of the daily temperatures differ by more than 1°C.

Table 1a lists the dates with the largest temperature anomalies in the five regions. It is apparent that there is only partial overlap between adjacent regions, even after allowing for 1–2-day differences due to the migration of the core of an air mass. The numbers of days in common between adjacent regions of the United States are 4 of 10 (MW and EC), 5 of 10 (EC and GC), and 6 of 10 (MW and GC). The two European regions (NE and WE) have only 3 of 10 dates in common.

Table 1a shows that the regional temperature anom-

alies are larger in the United States than in the European regions. This tendency is especially evident in the cases of the 8th–10th ranked anomalies, which are nearly twice as large in the United States as in Europe. These results imply that the North American regions are more susceptible to large negative temperature anomalies (−15° to −20°C) than their European counterparts. Table 2 contains the actual temperatures for the MW and WE regions from the years 1979–93, which are common to the NCEP and ECMWF reanalyses. The degree of similarity of corresponding temperatures from the two reanalyses implies that many of the ranks of the extreme dates would shift slightly, but that the overall suite of extreme events would remain quite similar, if based on a different reanalysis. In four of the five regions, the single most extreme date remains the same regardless of the reanalysis. Although the corresponding temperature anomalies from the two reanalyses generally differ by a degree or so, both reanalyses show that the extreme daily temperature anomalies are colder by 10°–18°C in the United States than in Europe. The relative extremity of the North American regional temperatures is enhanced by 1) the smaller areal fractions of water in the North American regions and 2) the smaller sizes of the North American regions. The differences in size do not change the fact that the actual minimum temperatures were more extreme *locally* in North America, as were the maximum magnitudes of the *local* anomalies.

Tables 1b and 1c indicate how the suites of extreme dates change if the selection is based on 3-day and 5-day averaged anomalies rather than single-day anomalies. The lengthening of the averaging period from 1–5 days often results in shifts of several ranks, especially in the lower portion of each list. In some cases, a date is displaced from a list by another date that had fallen just short of inclusion when an alternative averaging period was used. The lists from the 1-day and 5-day averaging procedures have the following numbers of dates in common: 5 of 10 in MW, 8 of 10 in EC, 5 of 10 in GC, 7 of 10 in NE, and 9 of 10 in WE.

## 5. Temporal distribution of extreme events

Before addressing the decadal variations of the extreme events, several winters deserve mention because of their multiple events. The winter of 1962–63 provided three of the top 10 entries for the Western Europe region on each of the three lists (1-day, 3-day, and 5-day events) in Table 1. This winter is widely regarded as the coldest of the past half-century, and perhaps of the entire twentieth century, in the United Kingdom (e.g., Thompson 1987). Interestingly, this winter also appears at least once on each of the North American lists, and it even appears multiple times on the list of the 10 coldest single days in both the East Coast (EC) and Gulf Coast (GC) regions. The Northern European region, on the other hand, experienced 3 of its 10 coldest events in January–February 1985. This same winter also

TABLE 1. Largest negative anomalies of regionally averaged temperatures based on (a) 1-, (b) 3-, and (c) 5-day running means. In (b) and (c), center dates of 3- and 5-day periods are listed.

| MW | | EC | | GC | | NE | | WE | |
|---|---|---|---|---|---|---|---|---|---|
| (a) 1-day criterion | | | | | | | | | |
| 22 Dec 89 | −22.5°C | 25 Dec 83 | −19.0°C | 23 Dec 89 | −21.2°C | 10 Jan 87 | −15.4°C | 12 Jan 87 | −12.8°C |
| 24 Dec 83 | −20.6 | 21 Jan 85 | −18.8 | 25 Dec 83 | −19.8 | 30 Dec 78 | −14.6 | 02 Feb 56 | −11.5 |
| 03 Feb 96 | −19.9 | 19 Jan 94 | −18.6 | 21 Jan 85 | −19.6 | 03 Feb 66 | −13.2 | 01 Feb 54 | −9.1 |
| 15 Jan 72 | −18.3 | 23 Dec 89 | −18.3 | 13 Dec 62 | −17.6 | 09 Feb 85 | −11.3 | 07 Jan 85 | −8.9 |
| 20 Jan 85 | −18.1 | 17 Jan 77 | −16.7 | 30 Jan 66 | −17.3 | 21 Jan 85 | −10.6 | 23 Dec 62 | −8.7 |
| 04 Feb 89 | −17.7 | 22 Feb 63 | −16.4 | 11 Jan 82 | −16.8 | 16 Dec 78 | −10.5 | 09 Feb 86 | −8.6 |
| 13 Nov 86 | −17.7 | 04 Feb 96 | −16.4 | 02 Feb 51 | −16.5 | 06 Jan 50 | −10.3 | 05 Mar 71 | −8.6 |
| 17 Nov 59 | −17.1 | 17 Feb 58 | −16.2 | 04 Feb 96 | −16.4 | 05 Jan 85 | −10.3 | 13 Jan 63 | −8.6 |
| 29 Jan 66 | −16.8 | 13 Dec 62 | −16.2 | 24 Jan 63 | −15.7 | 14 Feb 79 | −9.8 | 07 Feb 91 | −8.3 |
| 24 Jan 63 | −16.5 | 02 Mar 80 | −15.9 | 11 Jan 62 | −15.3 | 31 Jan 56 | −9.7 | 02 Feb 63 | −8.2 |
| (b) 3-day criterion | | | | | | | | | |
| 24 Dec 83 | −19.9°C | 23 Dec 89 | −16.5°C | 23 Dec 89 | −18.7°C | 10 Jan 87 | −14.5°C | 12 Jan 87 | −11.3°C |
| 22 Dec 89 | −19.8 | 25 Dec 83 | −15.6 | 25 Dec 83 | −16.6 | 30 Dec 78 | −13.4 | 02 Feb 56 | −10.2 |
| 03 Feb 96 | −18.3 | 04 Feb 96 | −15.2 | 04 Feb 96 | −14.3 | 03 Feb 66 | −11.9 | 01 Feb 54 | −8.9 |
| 04 Feb 89 | −15.2 | 18 Feb 58 | −15.2 | 11 Jan 62 | −13.6 | 08 Feb 85 | −10.6 | 07 Jan 85 | −8.7 |
| 29 Jan 66 | −15.1 | 20 Jan 94 | −14.7 | 22 Jan 85 | −13.6 | 06 Jan 50 | −9.8 | 05 Mar 71 | −8.4 |
| 11 Mar 98 | −14.7 | 18 Jan 77 | −14.6 | 13 Dec 62 | −13.4 | 06 Jan 85 | −9.6 | 24 Dec 62 | −8.3 |
| 24 Jan 63 | −14.4 | 02 Mar 80 | −14.3 | 18 Jan 77 | −13.3 | 21 Jan 85 | −9.4 | 03 Feb 63 | −8.0 |
| 03 Nov 91 | −14.3 | 13 Dec 62 | −13.6 | 09 Mar 96 | −12.6 | 16 Dec 78 | −9.1 | 13 Jan 63 | −7.7 |
| 28 Feb 62 | −14.2 | 11 Jan 82 | −13.1 | 03 Feb 51 | −12.1 | 02 Mar 87 | −8.7 | 09 Feb 86 | −7.6 |
| 17 Feb 58 | −14.0 | 21 Jan 85 | −12.7 | 17 Feb 58 | −12.1 | 30 Jan 56 | −8.7 | 07 Feb 91 | −7.4 |
| (c) 5-day criterion | | | | | | | | | |
| 24 Dec 83 | −17.9°C | 23 Dec 89 | −14.1°C | 23 Dec 89 | −15.1°C | 09 Jan 87 | −13.7°C | 13 Jan 87 | −9.9°C |
| 02 Feb 96 | −17.3 | 25 Dec 83 | −12.8 | 25 Dec 83 | −13.3 | 30 Dec 78 | −11.9 | 02 Feb 56 | −8.4 |
| 21 Dec 89 | −17.1 | 04 Feb 86 | −12.7 | 03 Feb 86 | −11.3 | 04 Feb 66 | −10.0 | 07 Jan 85 | −8.2 |
| 25 Jan 63 | −13.2 | 18 Feb 58 | −12.6 | 18 Feb 58 | −11.3 | 08 Feb 85 | −9.8 | 02 Feb 54 | −8.1 |
| 05 Feb 89 | −12.9 | 18 Jan 94 | −12.2 | 11 Jan 62 | −10.7 | 08 Jan 50 | −9.6 | 02 Feb 63 | −7.9 |
| 31 Jan 51 | −12.7 | 18 Jan 77 | −12.0 | 18 Jan 77 | −10.6 | 06 Jan 85 | −8.9 | 25 Dec 62 | −7.7 |
| 04 Mar 60 | −12.5 | 12 Dec 62 | −11.5 | 10 Mar 96 | −10.5 | 01 Mar 71 | −8.3 | 05 Mar 71 | −7.4 |
| 09 Dec 72 | −12.2 | 01 Mar 80 | −11.1 | 13 Jan 82 | −10.3 | 21 Jan 85 | −8.1 | 30 Dec 96 | −7.3 |
| 02 Feb 85 | −12.2 | 09 Jan 70 | −10.6 | 08 Jan 70 | −10.0 | 02 Mar 87 | −8.0 | 20 Jan 63 | −7.3 |
| 17 Feb 58 | −12.2 | 22 Jan 70 | −10.6 | 05 Mar 60 | −10.0 | 10 Jan 68 | −7.9 | 09 Feb 86 | −6.8 |

appears on each of the single-day lists for the North American regions. While these outstanding years suggest that extreme cold can affect both sides of the Atlantic in the same year, the North American lists do not show the single-year "clusters" of events to the extent that the European regions do. The implication is that persistent cold during a single winter may be less common in the United States than in Europe, although it must be noted that the sample of these exceptional single-year clusters in Europe is small.

Figure 2 summarizes the decadal frequencies of the extreme cold outbreaks listed in Table 1. (For the construction of Fig. 2, each event in Table 1 is counted once, but not more than once if its center date falls within one week of a previously counted event.) It is apparent that there is no trend toward fewer extreme cold events in the North American regions. The largest number of North American events occurred during the 1980s and the 1960s, and the smallest number during the 1950s. The final decade, 1990–99, is tied with the 1970s. The 1980s and 1960s also stand out as the decades with the most extreme cold events in Europe, although the 1990s emerge as the decade with the fewest occurrences in Europe. Thus, despite the recent trend toward higher mean minimum temperatures noted earlier, neither the North American nor the European areas examined here have seen a corresponding trend in the frequencies of extreme cold events.

TABLE 2. Comparison of temperatures from NCEP–NCAR and ECMWF reanalysis for major cold outbreaks during 1979–93.

| MW region | | | WE region | | |
|---|---|---|---|---|---|
| Date | $T_{NCEP}$ | $T_{ECMWF}$ | Date | $T_{NCEP}$ | $T_{ECMWF}$ |
| 22 Dec 89 | −25.2°C | −26.7°C | 12 Jan 87 | −10.2°C | −9.2°C |
| 24 Dec 83 | −23.7 | −24.7 | 09 Feb 86 | −5.6 | −6.0 |
| 20 Jan 85 | −21.6 | −24.5 | 07 Jan 85 | −6.1 | −7.2 |
| 04 Feb 89 | −20.3 | −19.9 | 07 Feb 91 | −5.2 | −5.6 |
| 13 Nov 86 | −11.7 | −14.5 | 02 Jan 79 | −5.1 | −3.9 |

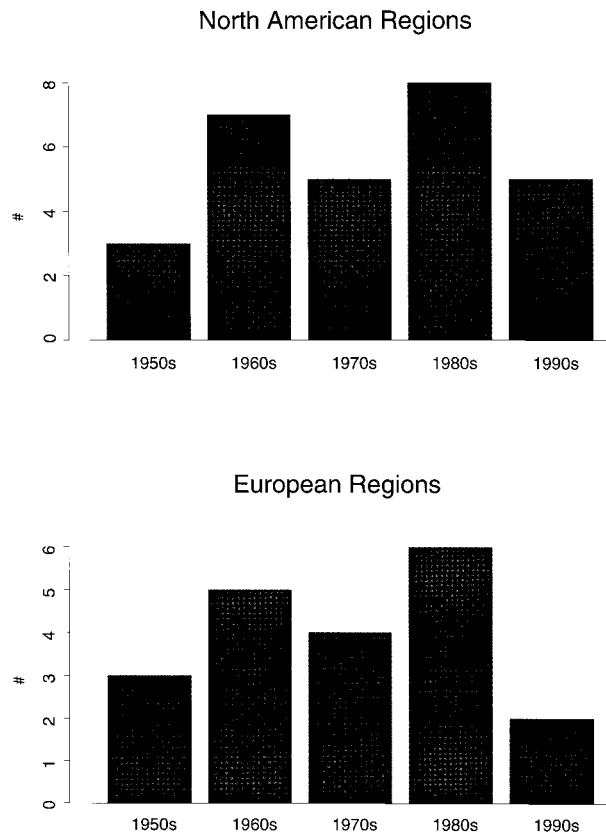North American Regions



European Regions



FIG. 2. Decadal distribution of the major cold events in (top) North American regions and (bottom) European regions.

Our conclusion about the absence of trends may nevertheless be dependent on the period examined in this study. The period from the 1930s to the 1950s is known to have been relatively warm over the Northern Hemisphere land areas, as it followed a warming from the century's early decades (IPCC 1996). Figure 3 shows the coldest single-day events dating back to the late 1800s at a single station (Urbana, IL: 40.1°N, 88.2°W) in the MW region. There is indeed an absence of extreme cold from the late 1930s to the early 1960s. However, the late 1890s and the first few decades of the 1900s are well populated by extreme cold days. Rogers and Rohli's (1991) finding that more Florida citrus freeze events occurred around the 1890s and after 1977 is consistent with the Urbana record. The absence of notable trends in the frequency of severe cold events within the past 2–3 decades as noted by Kunkel et al. (1999) is also supported by the temporal distributions in Figs. 2 and 3. Hence it appears that the frequency of extreme cold outbreaks over the United States may be characterized by low-frequency (multidecadal) variations, implying that trend assessments based on only several decades of data must be made with caution. Low-frequency variations in the severity of winters over western Europe (specifically, southern England) have also been suggested by Selfe (1970).

## 6. Spatial characteristics and evolution of cold events

The large temperature anomalies addressed here are associated with cold polar air masses, which can range up to several thousand kilometers in scale. As an illustration of the scale of the cold air outbreaks, Fig. 4a is a composite of the temperature anomalies based on the five highest-ranking single-day events in the MW region of the United States (cf. Table 1a). Not surprisingly, the largest anomalies are found over the midwestern portion of the United States; the magnitudes of the anomalies exceed 20°C in this area. When the single-day temperatures are first normalized by the standard deviations of the daily temperatures and then composited, the composite anomalies exceed three standard deviations in the MW region, as shown in Fig. 4b. The negative anomalies cover most of the United States and the southern half of Canada, indeed showing the several-thousand-kilometer scale characteristic of large air masses. Although the temperature anomalies of the airmasses contributing to Fig. 4 vary somewhat in size and location of the largest anomaly, the area inside the two-standard-deviation contour of Fig. 4b covers half the contiguous United States as well as part of south-central Canada. Hence the air masses are large in scale and share much of the same geographical coverage. The scales and normalized magnitudes of the composites for the other regions are similar, although the actual magnitudes of the composite anomalies for the European regions are smaller. Thus the events identified here are spatially extensive features with anomalies exceeding several standard deviations over a substantial portion of the region under consideration.

In order to determine the origins of the cold air responsible for the large anomalies, back-trajectories were evaluated using the three-dimensional winds in the reanalysis output. The origin of each back-trajectory was a point 50 mb above the surface ($\sigma = 0.95$) at the location of the largest negative temperature anomaly on the center date of the cold event in a particular region. The trajectories were computed using 1-h time steps. The hourly winds were interpolated linearly from the 6-h reanalysis. For each 1-h increment, the horizontal and vertical velocities at the nearest grid point to the position of the air parcel were used to move the parcel back to a location for the next (farther back in time) 1-h timestep. Each trajectory was plotted at 6-h intervals extending back through the 12 days prior to the arrival of the cold parcel at its destination 50 mb above the surface in the appropriate region of the United States or Europe. Thus each trajectory plot consists of 48 points, each of which differs horizontally and vertically from its prior and subsequent positions according to the local winds at the corresponding time.

Figure 5 shows a sample of six North American trajectories, two for each of the three regions in the United States. The trajectories are for temporally distinct events
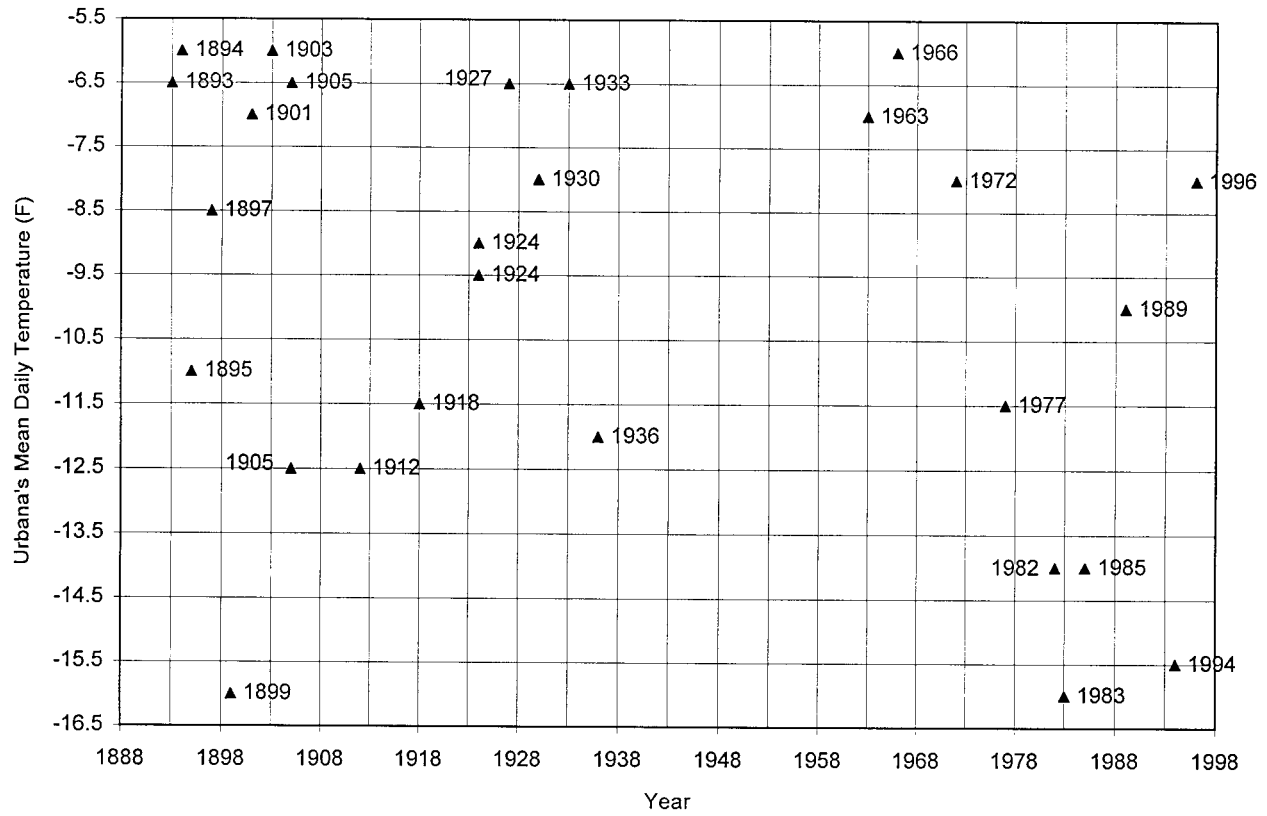
FIG. 3. Years of days with lowest daily mean temperatures at Urbana, IL. Daily temperatures are plotted on *y* axis, colder downward.
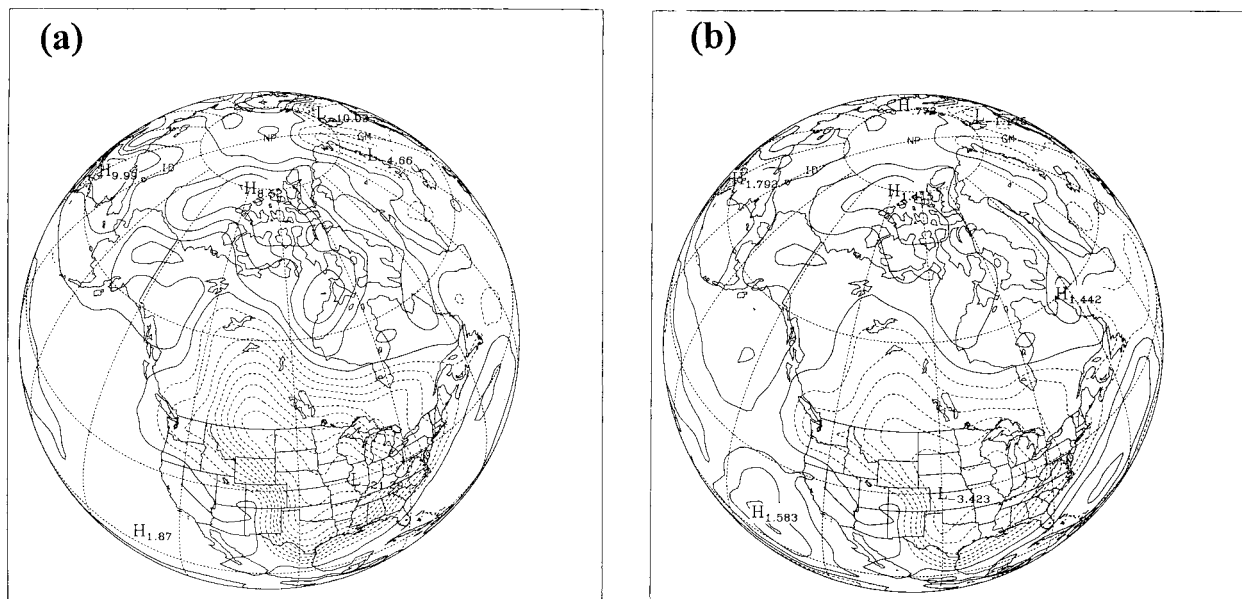


FIG. 4. (a) Surface air temperatures (°C) composited over five coldest days in MW region (Table 1a), and (b) corresponding normalized values (units: std dev of daily temperature).
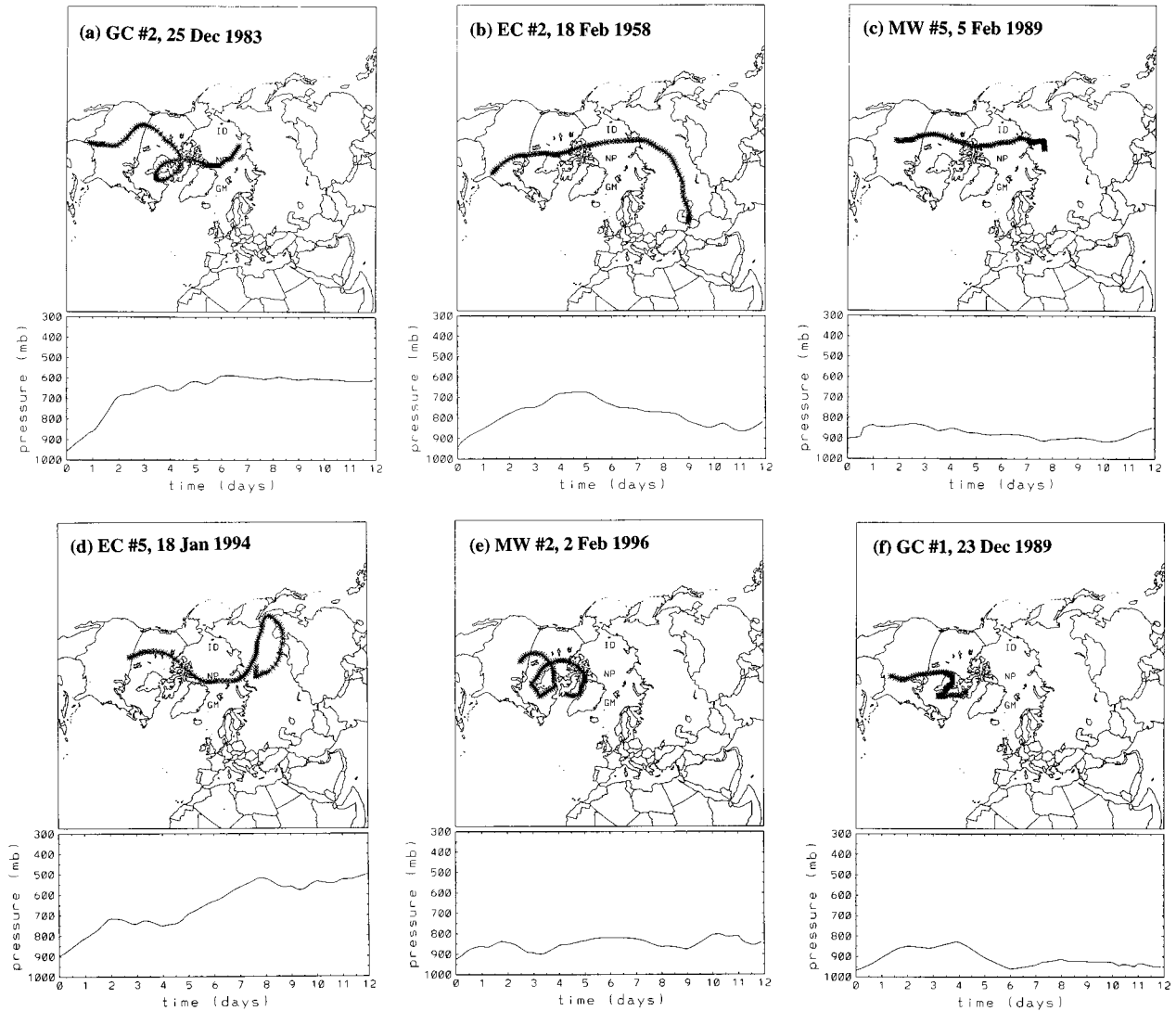
FIG. 5. Trajectories (horizontal views in upper panels, vertical views in lower panels) of air reaching a point 50 mb above surface on center days of the following major North American cold events from Table 1c: (a) GC #2, 25 Dec 1983; (b) EC #2, 18 Feb 1958; (c) MW #5, 5 Feb 1989; (d) EC #5, 18 Jan 1994; (e) MW #2, 2 Feb 1996; (f) GC #1, 23 Dec 1989.

selected from the five most extreme events listed in the North American columns of Table 1c. It is apparent that the core of the cold air reaches the affected region from the north or northwest. The most common origins of the trajectories (including those not shown in Fig. 5) are the northern fringes of North America (e.g., Fig. 5f), the Arctic Ocean (e.g., Fig. 5a), northern Asia (e.g., Fig. 5c), and the subpolar seas of the North Atlantic (e.g., Fig. 5e). Many of the trajectories suggest stagnation or slow movement over northwestern Canada, where the snow-covered terrestrial surface and minimal solar radiation are conducive to diabatic cooling of the low-level air. Figure 5 also shows that the air parcels undergo subsidence during their southward trajectory toward middle latitudes. The subsidence, which is consistent with the proximity of a high pressure center at the core

of the cold air mass, typically results in 100–300 mb of descent, although Figs. 5a and 5d show that the descent can be considerably greater if the trajectory extends back to the Asian side of the Arctic. Trajectories such as the latter suggest that the parcels were in other synoptic systems prior to their entrainment into the cold polar air masses. The 100–300 mb magnitudes of subsidence typical of most trajectories indicate that the air near the surface would have been even colder than it was if it were not for the adiabatic warming associated with the subsidence.

Figure 6 shows that subsidence also characterizes the European trajectories. However, a fundamental difference in the European trajectories is their indication of source regions to the east, particularly over northern Asia. The westward motion of the cold airmass cores
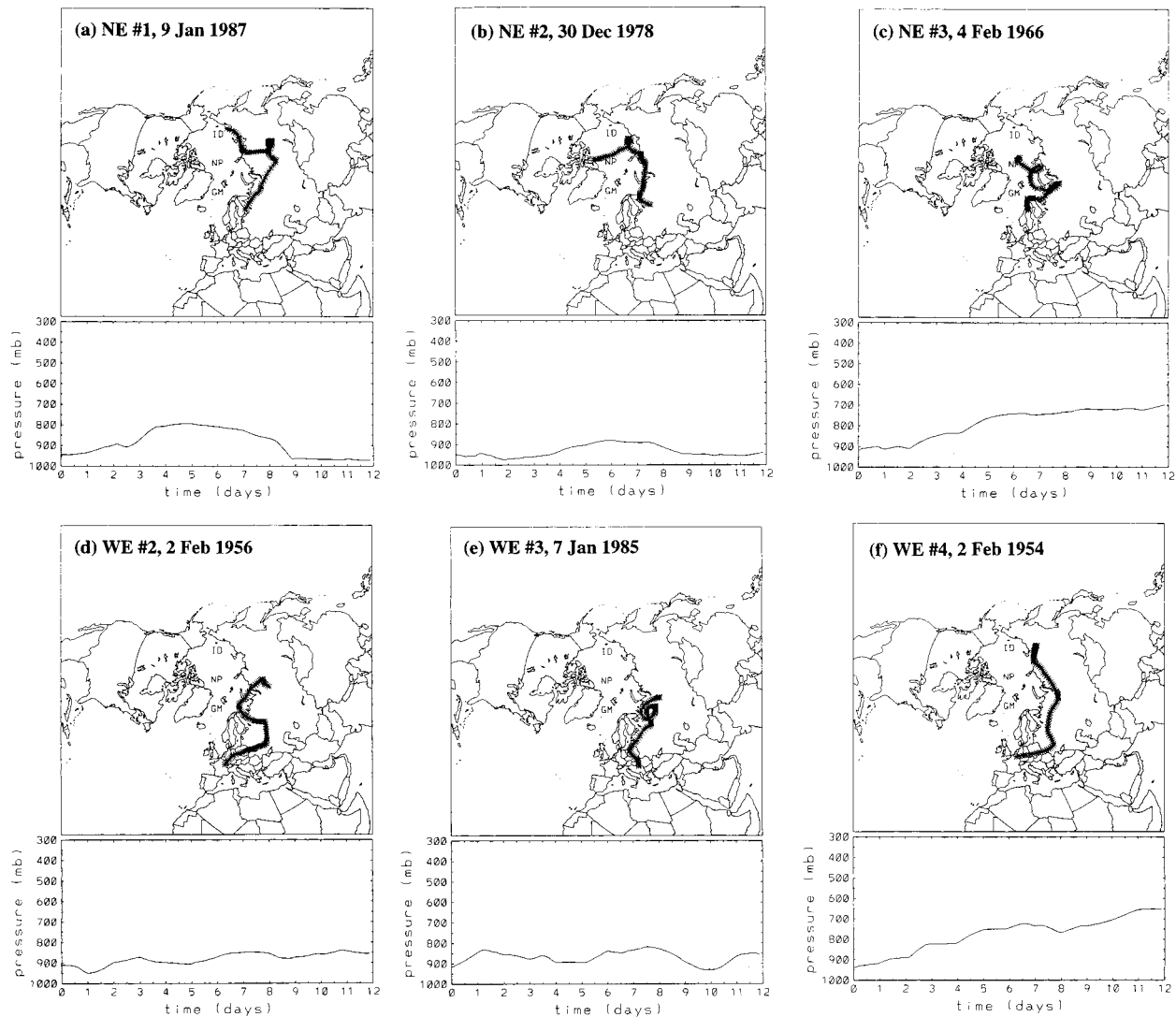
FIG. 6. As in Fig. 5, but for the following major European cold events: (a) NE #1, 9 Jan 1987; (b) NE #2, 30 Dec 1978; (c) NE #3, 4 Feb 1966; (d) WE #2, 2 Feb 1956; (e) WE #3, 7 Jan 1985; (f) WE #4, 2 Feb 1954.

contrasts with the southward or southeastward movement of the cold air masses affecting the United States. In many of the European trajectories, there are indications of stagnation over the western Siberian sector of Russia, not unlike the stagnation of the North American trajectories over northwestern Canada. The westward migration of the European cold outbreaks suggests that the likelihood of such an outbreak is tied directly to the intensity of the eastward airflow reaching Europe from the North Atlantic. The NAO index is a natural measure of this intensity.

In order to examine more comprehensively the temporal evolution and spatial teleconnections associated with the cold outbreaks, we constructed composite anomaly fields of sea level pressure (SLP) for various times prior to the arrival of the core of the cold air masses in their respective midlatitude regions. The in-

puts to the composite anomaly fields were the sea level pressure fields from the 10 most extreme events listed in a particular column of Table 1c, for which the event identification was based on 5-day running mean temperature anomalies in a particular region. The pressure anomaly composites were constructed for the dates listed in Table 1c ("Day-0"), and for the dates 2 days earlier ("Day-2"), 4 days earlier ("Day-4"), . . . , and 12 days earlier ("Day-12"), thereby permitting examinations of the evolution of the SLP anomalies over the 12 days prior to each region's coldest days.

Figure 7 shows the composite SLP anomalies on Day-10, Day-6, Day-2, and Day-0 for the MW region of the United States. Ten days prior to the outbreak, there are modest positive anomalies over the Arctic Ocean and northwestern North America, together with negative anomalies over the eastern North Atlantic and the west-
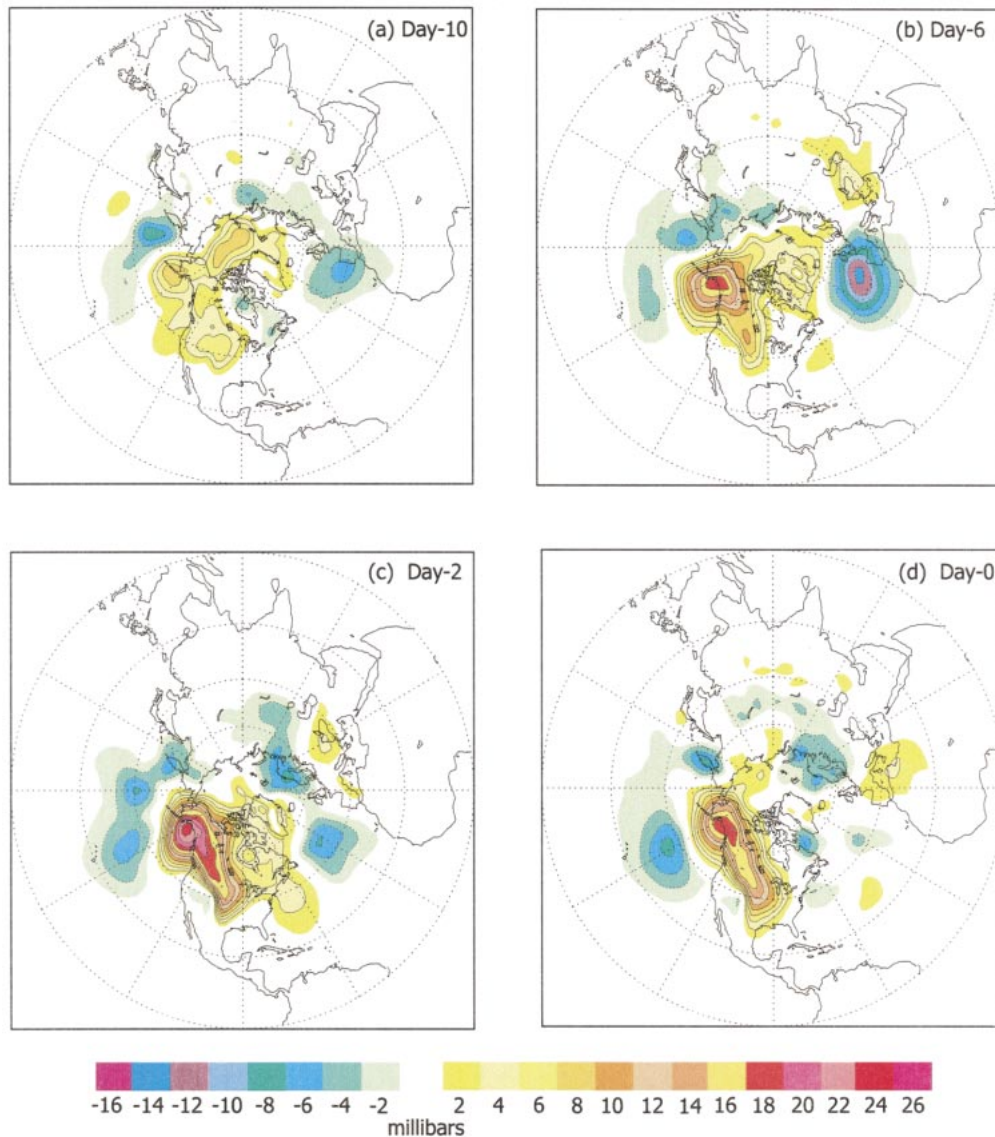
FIG. 7. SLP anomaly composites for (a) 10 days, (b) 6 days, (c) 2 days, and (d) 0 days prior to the dates of the 10 cold events in the Midwest (MW) region. Numbers below color bar denote the lower limit of each 2-mb range of magnitudes. Unshaded areas have magnitudes smaller than 2 mb.

ern Bering Sea. This pattern intensifies by Day-6, as the positive anomalies near the Alaska/Yukon border approach 20 mb. The negative anomalies of up to −15 mb offshore of southern Europe, in conjunction with positive anomalies over the subpolar North Atlantic, result in a pattern that would project highly onto the negative phase of the NAO and the Arctic oscillation. By Day-2, the positive anomalies over Alaska and western Canada become the dominant feature, which spreads southeastward. The values of approximately +25 mb in the Alaskan core on Day-2 represent impressive and highly significant anomalies for a composite based on 10 different cases selected on the basis of subsequent temperatures thousands of km to the southeast. (The $t$-values of the Alaskan composite anomalies in Fig. 7c

exceed the 98% significance thresholds for a sample size of 10.) The pressure-temperature linkage is apparent in the strength of the implied anomalies of northwesterly gradient winds on the forward side of the largest SLP anomalies. The airflow directly from the Arctic to the Midwestern United States is strikingly apparent on Day-0.

Figure 8 shows the corresponding sequence of SLP anomaly patterns for the EC region. (The patterns for the EC and GC regions are sufficiently similar that the following discussion applies to the GC as well as the EC region.) The outstanding feature of the Day-10 field is a strong signature of the negative phase of the North Atlantic and Arctic oscillations: composite anomalies of −15 mb and +13 mb are found in the subtropical At-
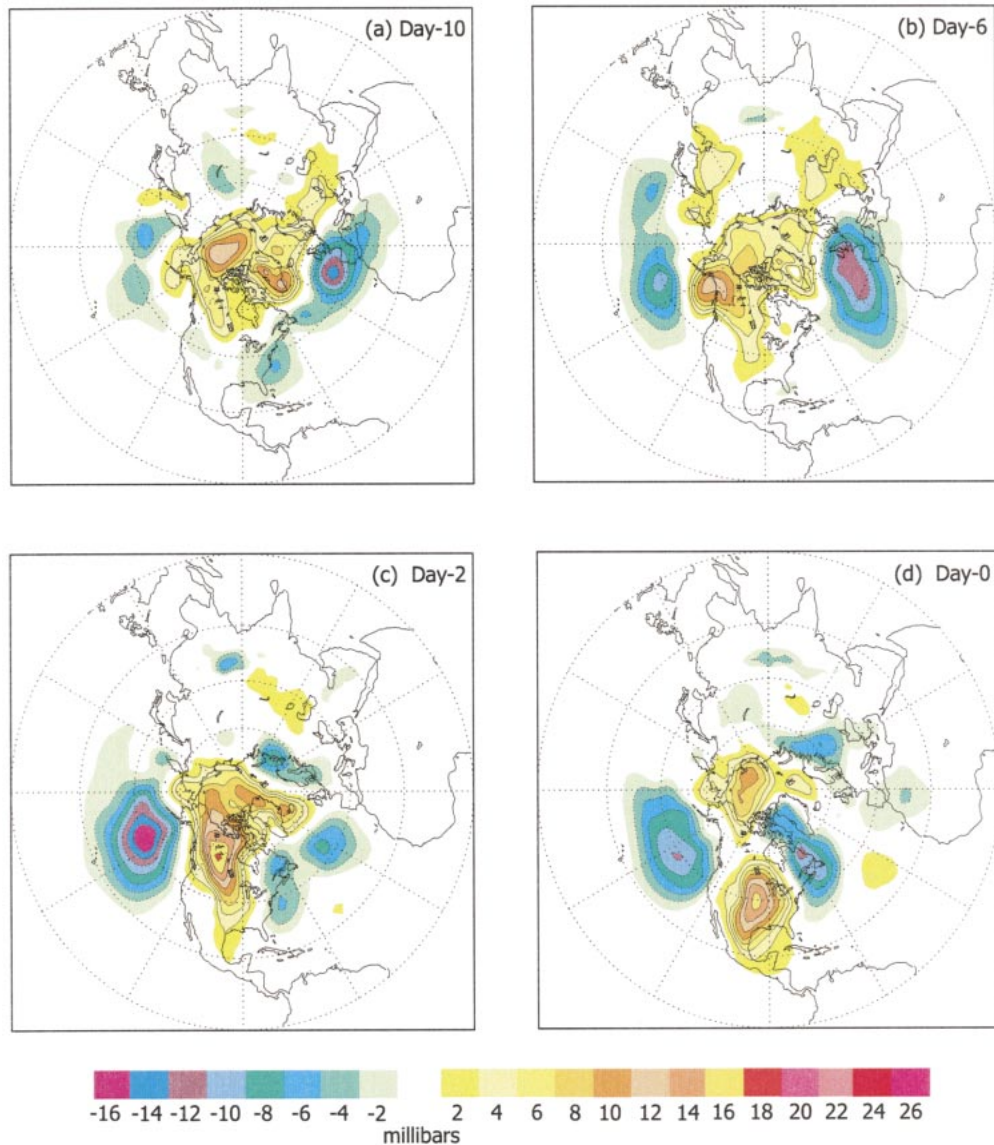
FIG. 8. As in Fig. 7, but for the East Coast (EC) region.

lantic (offshore of Portugal) and the subpolar North Atlantic, respectively. The subtropical Atlantic feature expands considerably by Day-6, and subsequently weakens, while the positive anomaly strengthens and moves through northwestern North America on Day-2. A strong negative anomaly develops in the North Pacific by Day-6, resulting in a well-developed signature of the North Pacific oscillation (NPO). This signature transitions to a sea-level manifestation of the Pacific–North American teleconnection by Day-2, when the negative anomaly in the North Pacific and the positive anomaly over western Canada have magnitudes of −17 mb and +19 mb, respectively. Figures 7 and 8 together imply that common features of the MW and EC outbreaks are antecedent negative NAO signatures, and a subsequent positive NPO-to-PNA evolution.

The primary differences between the MW and EC (also GC) composites are 1) the stronger negative anomalies over the oceans, and hence stronger NAO and NPO signatures, in the EC (GC) composites, and 2) the more southward migration of the positive SLP anomaly in the EC and GC cases. The EC and GC cases may be considered more dynamic in the sense that the positive anomaly remains over northwestern North America even at Day-0 in the MW case, while the anomaly center clearly detaches and moves southeastward by Day-0 to the contiguous United States in the EC and GC cases. This southeastward movement of the positive SLP anomalies is consistent with advection of the colder air into the more eastern (EC) and southern (GC) sectors of the country. Figures 8c and 8d also contain negative SLP anomalies over eastern North America, implying
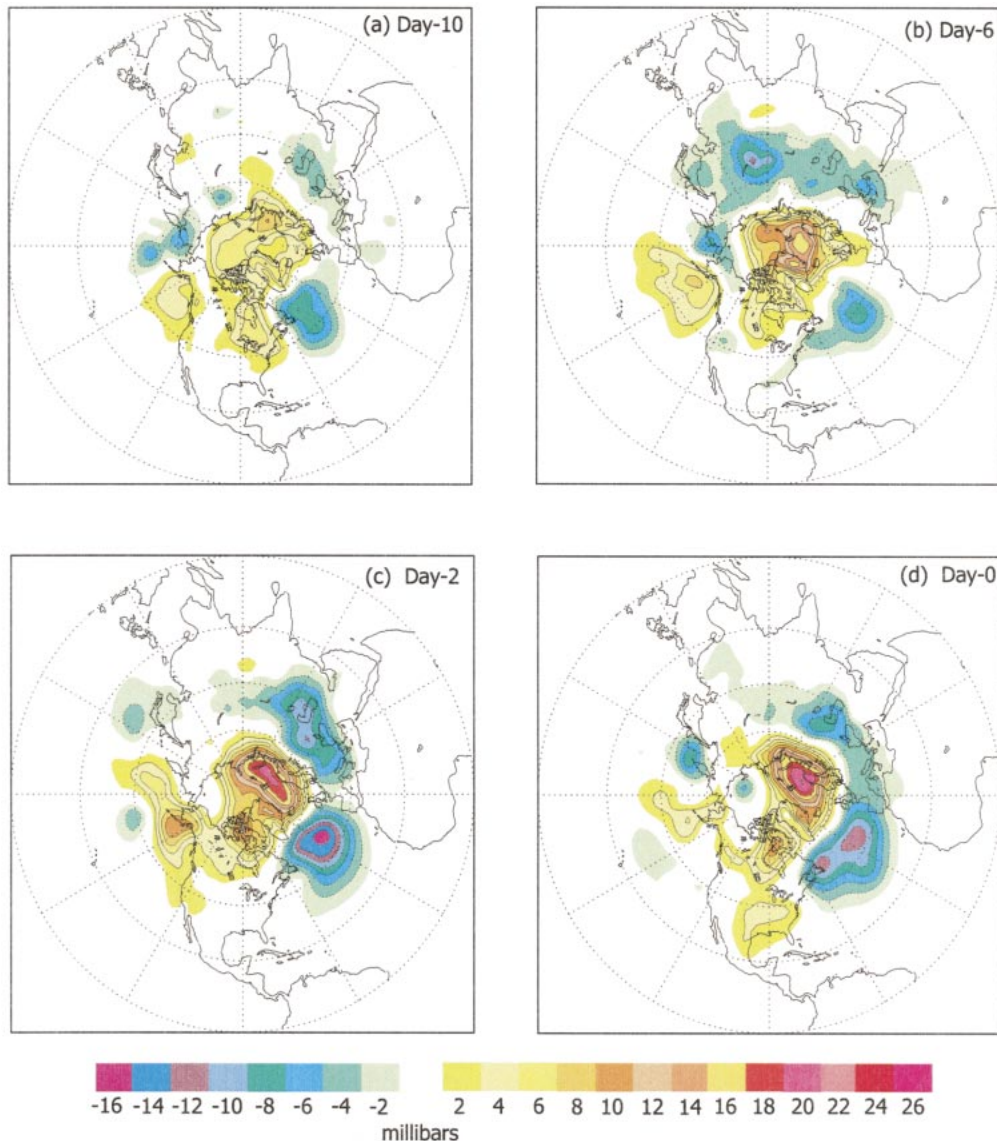
FIG. 9. As in Fig. 7, but for the Northern European (NE) region.

coastal cyclogenesis downstream of the cold air masses. This type of cyclogenesis was noted by Konrad and Colucci (1989) in their study of two cold outbreaks of January 1977.

The SLP anomaly patterns from which the European outbreaks evolve are very different from the patterns associated with the North American outbreaks, as one might expect from the earlier discussion of trajectories. Figure 9 shows that the Northern European events are preceded at Day-10 and Day-6 by a pattern of positive SLP anomalies over the Arctic and generally negative anomalies in the middle latitudes of the North Atlantic and Eurasia. This pattern evolves by Day-2 into a strong variant of the negative phase of the North Atlantic oscillation, with anomalies of $+22$ mb and $-16$ mb over the Norwegian–Barents Seas and the central North At-

lantic, respectively. While this couplet clearly implies a major reduction of the normal westerly winds reaching Europe, its projection onto standard indices of the NAO (e.g., the Lisbon–Azores $-$ Iceland pressure difference) would not be extremely strong because the anomaly centers are displaced considerably westward from the Lisbon–Azores region and northeastward from Iceland. The displacement of the positive anomaly center to the northern Scandinavian coastal region optimizes the eastward influx of cold Siberian air to Scandinavia and the remainder of northern Europe.

While the antecedent patterns for Western Europe (Fig. 10) show some similarity to those for Northern Europe, there are several differences. First, the primary lobe of negative anomalies in middle latitudes develops considerably farther to the east, over the Mediterranean
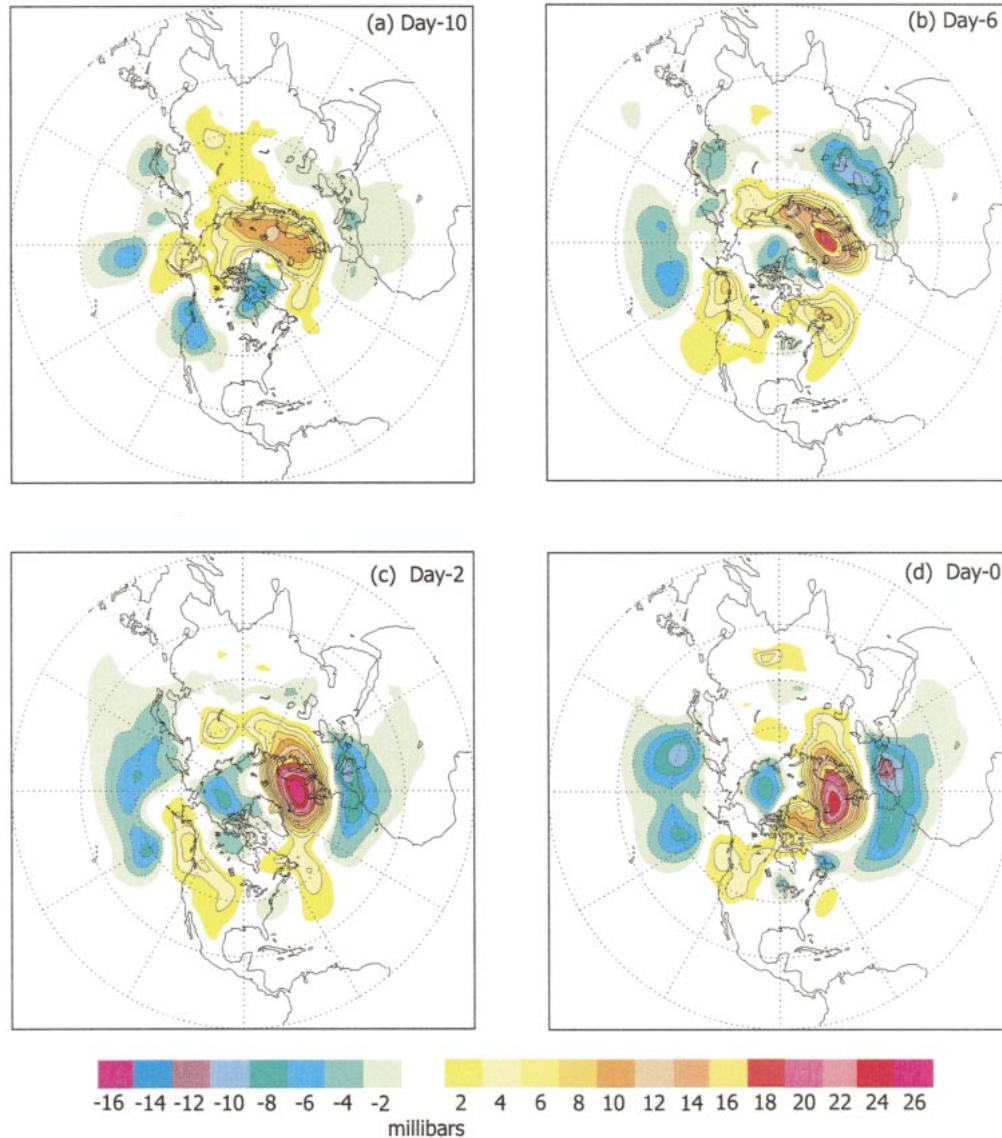
FIG. 10. As in Fig. 7, but for the Western European (WE) region.

region, rather than over the central North Atlantic as in the NE case. Second, the subpolar lobe of positive anomalies develops earlier, becomes stronger, and is centered farther south (between Iceland and Britain) in the WE case than in the NE case. The North Atlantic dipole at Day-2 and Day-0 in Fig. 10 would project strongly and negatively onto the standard NAO indices, especially because the composite SLP anomaly centers near Iceland have values exceeding +26 mb at Day-2 and +24 mb at Day-0. Although the NAO signature is strong in this case, again consistent with an extreme retardation (and even a reversal) of westerly airflow into Europe, the positive SLP anomalies do not extend into the Arctic Ocean. Hence, the projection onto the Arctic oscillation index of Thompson and Wallace (1998) will be much weaker than the projection onto the NAO.

In order to address the linkages to the NAO and the central Arctic more quantitatively, indices of the NAO and Arctic sea level pressure were composited over the 10 leading outbreaks (Table 1c) affecting each of the regions. The NAO index used here is based on nodal points that migrate seasonally to maximize the subpolar–subtropical correlation (Portis et al. 2001). (The nodal locations for the calendar months November–March are listed in Table 3.) Figure 11 shows the composite values of the NAO for each region's events and for the 12 days preceding the events. For all regions, the NAO is systematically negative in the period leading up to (and including) the cold outbreaks. The NAO values for the EC and GC regions of North America are more negative than −1.0 (standard deviations) for much of the antecedent week; the composite mean value

TABLE 3. Monthly nodal locations of the North Atlantic oscillation index for Fig. 11.

|  | Subpolar low | Subtropical high |
|---|---|---|
| Nov | 55°N, 35°W | 25°N, 47.5°W |
| Dec | 60°N, 20°W | 30°N, 30°W |
| Jan | 65°N, 20°W | 30°N, 20°W |
| Feb | 60°N, 35°W | 25°N, 37.5°W |
| Mar | 60°N, 50°W | 25°N, 40°W |

reaches—1.8 for the GC events at a lead time of six days. The negative values are consistent with the composite fields in Fig. 8 and with the positive correlations between winter-averaged values of the NAO index and temperatures in Florida (Downton and Miller 1993). For the European regions, the composite index values are generally between −0.25 and −1.00, although the values decrease to −1.8 for region WE over the few days immediately preceding the events. In this context, we reiterate that the centers of the SLP anomaly patterns most directly linked to the European outbreaks (Figs. 9–10) are generally displaced from the nodal points of the NAO, regardless of the definition of the NAO index. Nevertheless, it is apparent from Fig. 11 that cold out-

breaks over both continents are favored by the negative phase of the NAO.

Figure 12 is a similar summary of the antecedent Arctic pressure anomalies, defined here as the average of the gridded SLP anomalies over the region poleward of 70°N. This polar cap includes the Arctic Ocean and the northern portions of the North Atlantic subpolar seas. The plots for each region in Fig. 12 show that positive SLP anomalies in the central Arctic precede the cold outbreaks. Of the three North American regions, the EC shows the largest SLP anomalies (6–8 mb from Day-8 through Day-0), while the MW region shows the smallest anomalies, although the composite SLP anomaly for MW does reach +5.5 mb at Day-2. The plots in Fig. 12 for the two European regions show opposing temporal tendencies, consistent with the composite fields in Figs. 9–10. As the lead time for the Northern European region decreases from 12 to 0 days, the Arctic SLP anomaly increases from nearly zero to approximately 10 mb. The anomalies for the more southern WE region decrease from positive values of 5–6 mb at lead times of 8–12 days to values close to zero in the several days immediately prior to (and including) the major cold events. Thus the characteristics of the large-scale SLP
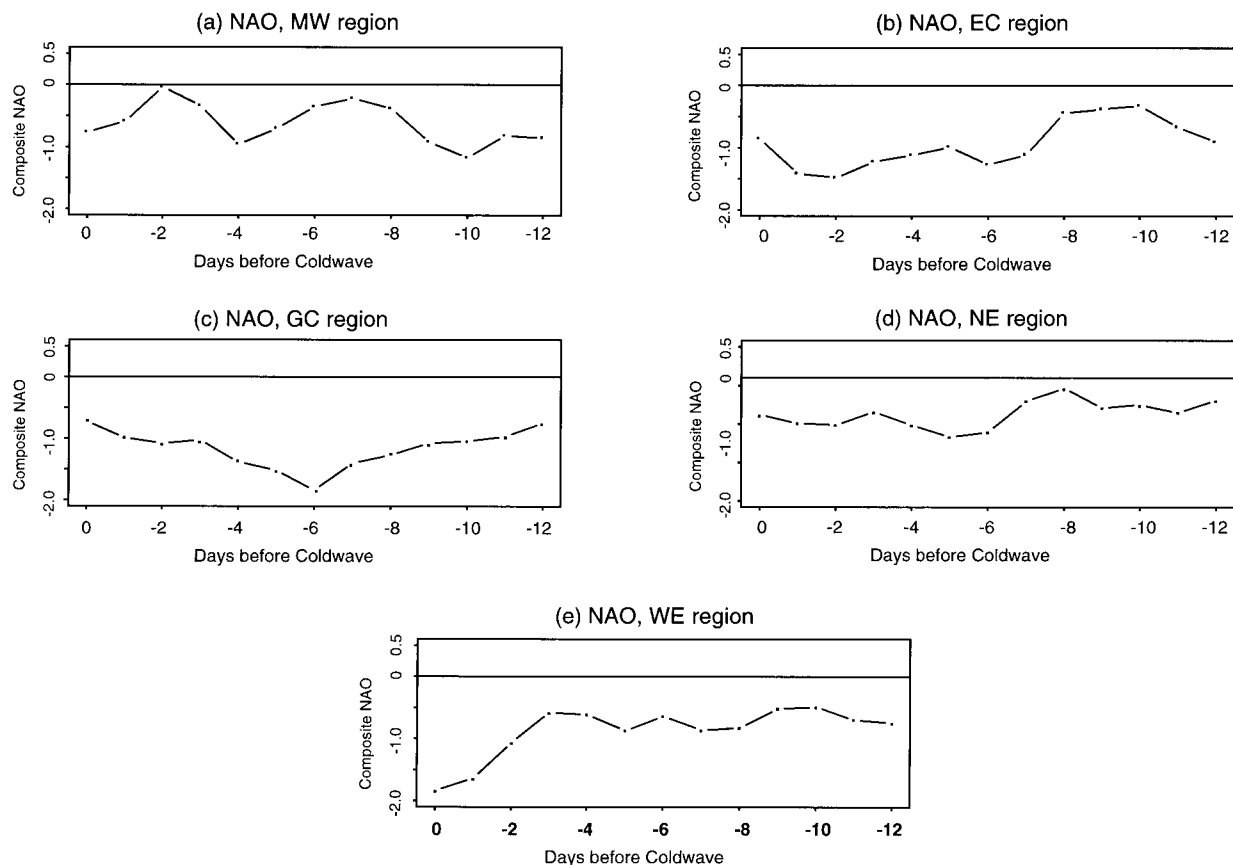


FIG. 11. Composite value of the NAO index during and prior to 10 coldest outbreaks in (a) MW region, (b) EC region, (c) GC region, (d) NE region, and (e) WE region. Composite values are plotted as functions of number of days (0, 1, 2, . . . , 12) prior to coldest days of events in Table 1c.
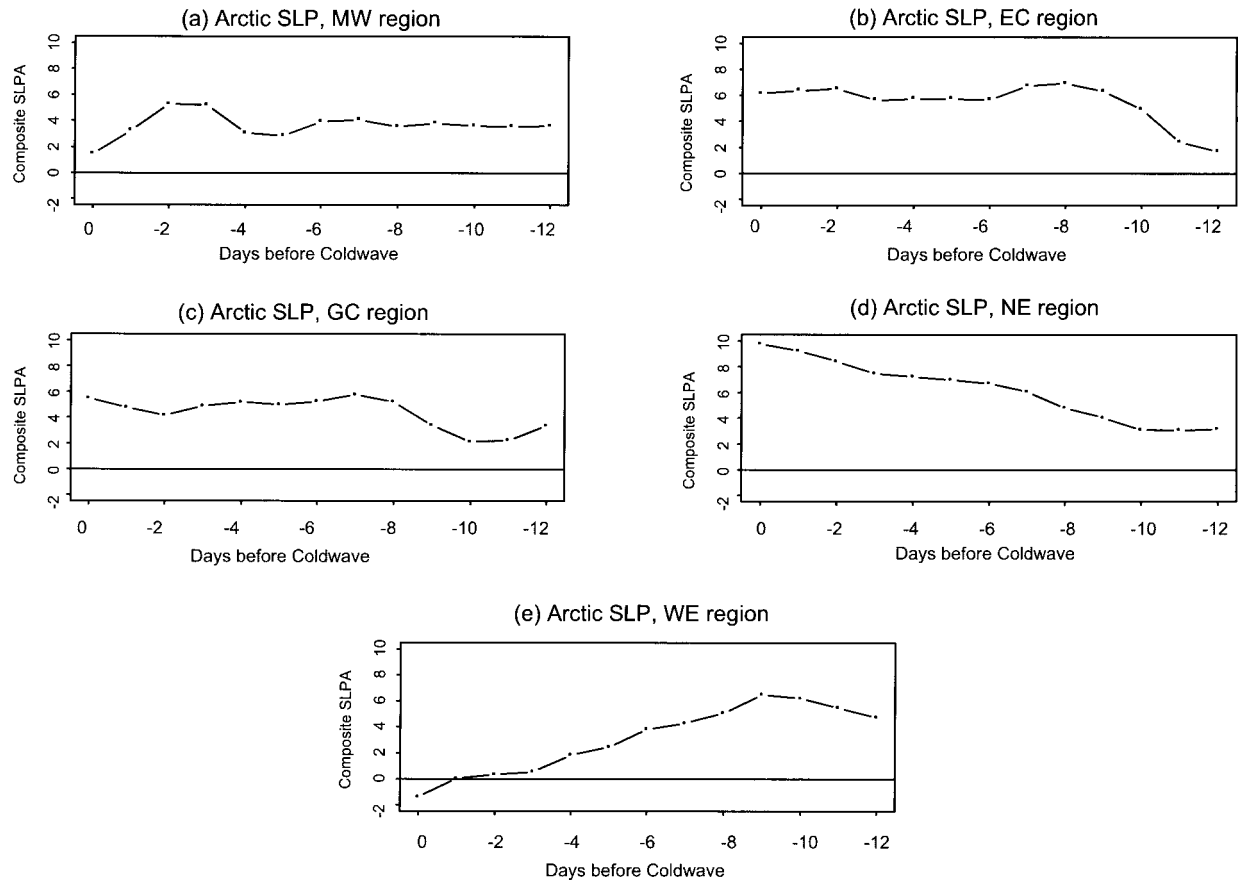
FIG. 12. As in Fig. 11, but for composite values of anomalies of sea level pressure (SLP) averaged over the central Arctic (70°–90°N).

anomaly pattern include positive pressure anomalies in the Arctic and negative NAO indices. While these two features imply consistent contributions to a negative Arctic oscillation index, the composite fields in Figs. 7–10 indicate that the relevant features in the North Atlantic and the Arctic often do not strengthen in phase and are often displaced geographically from the AO nodes of Thompson and Wallace (1998). Hence the AO index may not be the optimum indicator of an imminent cold outbreak over the 0–12 day timescale addressed here. The AO's linkage to temperature anomalies over longer timescales may well be stronger.

## 7. Conclusions

This assessment of major cold outbreaks over the past half-century leads to several conclusions, particularly with regard to differences between the North American and European cold events.

- The cold outbreaks affecting the United States are more extreme than those affecting Europe, in terms of both the actual air temperatures and the anomalies of air temperature.
- There is no apparent trend toward fewer extreme cold events on either continent, at least over the period

since 1948. Longer records remain to be investigated in this context.
- The trajectories of the coldest air are southward or southeastward over North America, but generally westward over Europe. Subsidence of several hundred millibars is typical of most trajectories of the coldest air to reach the surface in each region.
- Sea level pressure anomalies evolve consistently with the temperatures over the 1–2 weeks prior to the extreme cold outbreaks. Outbreaks affecting the East and Gulf Coasts of the United States appear to result from cold air "pools" that break off from high-latitude air masses; the Midwestern outbreaks appear to be more closely tied to the advection of cold air on the eastern side of air masses remaining in more northerly locations. Outbreaks over Western Europe and Northern Europe are distinguished by subtle locational differences of large anomalies of sea level pressure, but outbreaks affecting both regions involve the retardation and/or reversal of the North Atlantic westerlies impinging upon Europe.
- Negative values of the NAO index and positive anomalies of Arctic sea level pressures are features common to North American as well as European outbreaks. However, the strongest SLP anomaly features asso-

ciated with the outbreaks are generally shifted geographically relative to the nodal locations of the NAO and the Arctic oscillation.

There is a need to investigate further the linkage between the extreme outbreaks and the North Atlantic and Arctic oscillations by examining longer timescales and low-frequency variations of these (and other) teleconnection features. In this study, we have focused on the North Atlantic and Arctic associations because previous studies have emphasized associations between North American cold outbreaks and Pacific features (e.g., Rogers and Rohli 1991; Downton and Miller 1993).

An additional need is the extension of the trend analysis to include the decades prior to the start of the NCEP–NCAR reanalysis in 1948. The networks of historical stations in the United States and Europe are good (e.g., the Historical Climatology Network of the United States). The single-station results reported here suggest that extreme outbreaks may have been relatively frequent in the late 1800s and early 1900s, but the spatial representativeness of data from one station is open to question. Any such extension back beyond the 1940s will not have the benefit of the three-dimensional wind fields used in the present study.

Finally, there is a need for a diagnosis of the extreme airmass formation mechanisms in terms of the underlying physics (e.g., surface fluxes) and dynamics, particularly in the context of the frequent stagnation of the trajectories over northern land areas. The relative importance of thermodynamic and dynamic processes in the formation of extreme air masses is unclear. Colucci et al.'s (1999) assessment of cooling mechanisms in numerical weather prediction models suggests that adiabatic and diabatic processes can both contribute to the cooling to extreme temperatures. Because the reanalysis-derived surface fluxes are subject to large uncertainties at present, we have refrained from the inclusion of surface energetics in this study. As reanalysis-derived products improve, such studies will be feasible. One may also hypothesize that 1) an absence of cloudiness plays a role in the formation of the coldest air masses (Walsh and Chapman 1998), and 2) extensive snow cover favors the southward penetration of extremely cold air, in accordance with the results of Ellis and Leathers (1998). With regard to 1), Curry's (1983, 1987) model results indicate that low cloudiness and clear-sky ice-crystal precipitation can enhance near-surface cooling in high latitudes during winter, even to the extent that the diabatic cooling leads to the intensification of the surface anticyclone. Controlled experiments are needed for a more general characterization of the importance of this mechanism, as well as for tests of other hypotheses, and for case studies of some of the extreme cold events identified in this study. Such experiments may also provide a means to investigate possible feedbacks that may contribute to the clustering of extreme cold outbreaks in certain winters, for example, the winters of 1962–63 and 1984–85.

REFERENCES

Brázdil, R., and Coauthors, 1996: Trends of maximum and minimum daily temperatures in Central and Southeastern Europe. *Int. J. Climatol.,* **16,** 765–782.

Brugge, R., 1991: The cold snap of February 1991. *Weather,* **46,** 222–231.

Colle, B. A., and C. F. Mass, 1995: The structure and evolution of cold surges east of the Rocky Mountains. *Mon. Wea. Rev.,* **123,** 2577–2610.

Colucci, S. J., and J. C. Davenport, 1987: Rapid surface anticyclogenesis: Surface climatology and attendant large-scale circulation changes. *Mon. Wea. Rev.,* **115,** 822–836.

——, D. P. Baumhefner, and C. E. Konrad II, 1999: Numerical prediction of a cold-air outbreak: A case study with ensemble forecasts. *Mon. Wea. Rev.,* **127,** 1538–1550.

Curry, J., 1983: On the formation of continental polar air. *J. Atmos. Sci.,* **40,** 2278–2292.

——, 1987: The contribution of radiative cooling to the formation of cold-core anticyclones. *J. Atmos. Sci.,* **44,** 2575–2592.

Dallavalle, J. P., and L. F. Bosart, 1975: A synoptic investigation of anticyclogenesis accompanying North American polar air outbreaks. *Mon. Wea. Rev.,* **103,** 941–957.

DeGaetano, A. T., 1996: Recent trends in maximum and minimum temperature threshold exceedences in the northeastern United States. *J. Climate,* **9,** 1646–1660.

Downton, M. W., and K. A. Miller, 1993: The freeze risk to Florida citrus. Part II: Temperature variability and circulation patterns. *J. Climate,* **6,** 364–372.

Easterling, D. R., J. L. Evans, P. Y. Groisman, T. R. Karl, K. E. Kunkel, and P. Ambenje, 2000: Observed variability and trends in extreme climate events: A brief review. *Bull. Amer. Meteor. Soc.,* **81,** 417–425.

Ellis, A. W., and D. J. Leathers, 1998: A quantitative approach to evaluating the effects of snow cover on cold airmass temperatures across the U. S. Great Plains. *Wea. Forecasting,* **13,** 688–701.

Heino, R., and Coauthors, 1999: Progress in the study of climatic extremes in northern and central Europe. *Climatic Change,* **42,** 151–181.

Houghton, J. T., L. G. Meira Filho, B. A. Callander, N. Harris, A. Kattenberg, and K. Maskell, Eds., 1996: *Climate Change 1995: The Science of Climate Change.* Cambridge University Press, 572 pp.

Hurrell, J. W., and H. van Loon, 1997: Decadal variations in climate associated with the North Atlantic Oscillation. *Climatic Change,* **36,** 301–326.

Joung, C. H., and M. H. Hitchman, 1982: On the role of successive downstream development in East Asian polar air outbreaks. *Mon. Wea. Rev.,* **110,** 1224–1237.

Kalkstein, L. S., P. S. Dunne, and R. S. Vose, 1990: Detection of climatic change in the western North American Arctic using a synoptic climatological approach. *J. Climate,* **3,** 1153–1167.

Kalnay, E., and Coauthors, 1996: The NCEP/NCAR 40-Year Reanalysis Project. *Bull. Amer. Meteor. Soc.,* **77,** 437–471.

Karl, T. R., G. Kukla, V. N. Razuvaev, M. J. Changery, R. G. Quayle, R. R. Heim, D. R. Easterling, and C. B. Fu, 1991: Global warm-

ing: Evidence for asymmetric diurnal temperature change. *Geophys. Res. Lett.,* **18,** 2253–2258.

Konrad, C. E., II, 1996: Relationships between the intensity of cold-air outbreaks and the evolution of synoptic and planetary-scale features over North America. *Mon. Wea. Rev.,* **124,** 1067–1083.

——, and S. J. Colucci, 1989: An examination of extreme cold air outbreaks over eastern North America. *Mon. Wea. Rev.,* **117,** 2678–2700.

Kunkel, K. E., R. A. Pielke Jr., and S. A. Changnon, 1999: Temporal fluctuations in weather and climate extremes that cause economic and human health impacts: A review. *Bull. Amer. Meteor. Soc.,* **80,** 1077–1098.

Mogil, H. M., A. Stern, and R. Hagan, 1984: The great freeze of 1983: Analyzing the causes and the effects. *Weatherwise,* **37,** 304–308.

Portis, D. H., J. E. Walsh, M. El Hamly, and P. J. Lamb, 2001: Seasonality of the North Atlantic Oscillation. *J. Climate,* **14,** 2069–2078.

Quiroz, R. S., 1984: The climate of the 1983–84 winter—A season

of strong blocking and severe cold in North America. *Mon. Wea. Rev.,* **112,** 1894–1912.

Rogers, J. C., and R. V. Rohli, 1991: Florida citrus freezes and polar anticyclones in the Great Plains. *J. Climate,* **4,** 1103–1113.

Selfe, R. W., 1970: Periodicities in London winters. *Weather,* **25,** 374–378.

Thompson, D. W. J., and J. M. Wallace, 1998: The Arctic Oscillation signature in the wintertime geopotential height and temperature fields. *Geophys. Res. Lett.,* **25,** 1297–1300.

Thompson, R. D., 1987: Cold winters in southern England. *Weather,* **42,** 160–161.

Wagner, J. A., 1977: Weather and circulation of January 1977—The coldest month on record in the Ohio Valley. *Mon. Wea. Rev.,* **105,** 553–560.

Walsh, J. E., and W. L. Chapman, 1998: Arctic cloud–radiation–temperature associations in observational data and atmospheric reanalyses. *J. Climate,* **11,** 3030–3045.

Wexler, H., 1951: Anticyclones. *Compendium of Meteorology,* T. F. Malone, Ed., Amer. Meteor. Soc., 621–628.

Witten, D., 1981: Cold related fatalities increasing annually. *Weatherwise,* **34,** 260.